JARS Journal of Applied Remote Sensing

RESEARCH PAPER

Long-term evaluation of Landsat 9 OLI data product uniformity at focal plane module-boundaries using Earth scenes

Raviv Levy,[a,*] Cibele Teixeira Pinto,[a] Jeffrey A. Miller,[a] and Kurtis Thome[b]
[a]Science Systems and Applications, Inc., NASA/GSFC Code 618, Greenbelt, Maryland, United States
[b]NASA Goddard Space Flight Center, Greenbelt, Maryland, United States

ABSTRACT. The uniformity performance characteristic in remote sensing data products is a metric that helps evaluate how an image accurately represents radiometric responses to geophysical variability at the Earth's surface or within the atmosphere. These uniformity attributes are used in Earth remote sensing science applications such as investigating water quality, land-cover/land-use classifications, and crop health assessments. To ensure these applications perform effectively, it is crucial to maintain and regularly assess the uniformity of calibrated remote sensing data products. In the Landsat missions, data from the onboard radiometric reference Solar diffuser device are used as the standard approach to derive the calibration parameters, ensuring the maintenance of both absolute radiance and radiometric uniformity through quarterly updates. This publication presents an alternative approach that leverages Earth scene data to assess the on-orbit uniformity performance of the Landsat 9 (L9) mission. The analysis characterizes uniformity at a specific set of spatial positions (the focal-plane boundary zones) that are intrinsic to the Operational Land Imager (OLI) focal plane design. By employing these Earth data statistics, the article further explores the temporal trends in the radiometric uniformity results. The results shown in this article demonstrate that for pushbroom imaging design systems with staggered sensor chip focal plane architectures, the co-registered pixels, i.e., overlapping measurements of the same ground target viewed by different detectors, offer a self-contained mechanism for assessing product uniformity. Remarkably, this alternative approach achieves a level of radiometric quality comparable to that delivered by a stable, well-characterized onboard Solar diffuser calibration device. The findings demonstrate the potential and capability of such Earth scene statistics in maintaining radiometric uniformity in calibrated data products to better than 1% (1-sigma) throughout the mission's operational lifetime.

 [DOI: 10.1117/1.JRS.20.038502]

Keywords: uniformity; Operational Land Imager; Landsat 9; stability; trend

Paper 260298G received Apr. 10, 2026; revised Jun. 3, 2026; accepted Jun. 8, 2026; published Jul. 2, 2026.

1 Introduction

The uniformity performance characteristic in remote sensing data products helps evaluate how well an image represents the true radiometric response associated with geophysical variability at the Earth's surface or in the atmosphere. Such uniformity is essential for many Earth science applications, including water quality monitoring, land-cover and land-use classification, and crop

*Address all correspondence to Raviv Levy, raviv.levy@nasa.gov

Handling Editor: Craig Alexander Coburn, Associate Editor

1931-3195/2026/$28.00

health assessment. To ensure these applications perform effectively, it is crucial to maintain and regularly assess the uniformity of calibrated remote sensing data products. The Landsat missions use Solar diffuser data as the standard approach to derive the calibration parameters needed to maintain both absolute radiance and uniformity through quarterly updates. Ensuring radiometric uniformity is especially critical because even small detector-to-detector inconsistencies can propagate into downstream science products, leading to misclassification of surface features, biases in temporal trend analyses, and reduced confidence in applications such as land cover change detection and vegetation condition monitoring. However, Solar diffuser-based assessments alone cannot fully characterize uniformity under the diverse illumination, bidirectional reflectance distribution function (BRDF), and spectral conditions encountered in real Earth scenes. Moreover, missions without stable onboard calibration devices lack an equivalent reference altogether.

A specific subset of the low-frequency uniformity metrics, routinely extracted from Earth data by the USGS Landsat processing system, is called as the focal plane module (FPM) overlap residual nonuniformity. In this context, the term sensor chip assembly (SCA) is used interchangeably with FPM. The FPM overlap residual nonuniformity is a special case of the banding metric that occurs at specific spatial frequencies and spatial positions in the scene corresponding to the focal plane module boundaries. Evaluating this metric is achieved by computing the mean ratio and mean difference of the calibrated radiance from the L1T data product (consistent, orthorectified, calibrated, and terrain corrected with ground control) for all sets of geometrically co-registered pixel pairs produced by detectors located in two adjacent focal plane modules. This comprehensive analysis across all Earth scenes produces what is designated as the overlap statistics information. The detailed mathematical description of the overlap statistics is provided in the Algorithm Description Document and other references.[1,2] In those past publications, several uniformity metrics as well as an overview of the OLI instrument are provided. For both the Operational Land Imager (OLI) payloads of the Landsat 8 and Landsat 9 missions, the across-track uniformity evaluation metrics was defined at select spatial frequencies: the high frequency detector-to-detector uniformity (also known as streaking) as well as the lower spatial frequency uniformity called banding. Visual examples for both types of uniformity residual error are seen in the ocean scene of Fig. 1 as narrow along-track stripes (streaking) or wide bands of visual

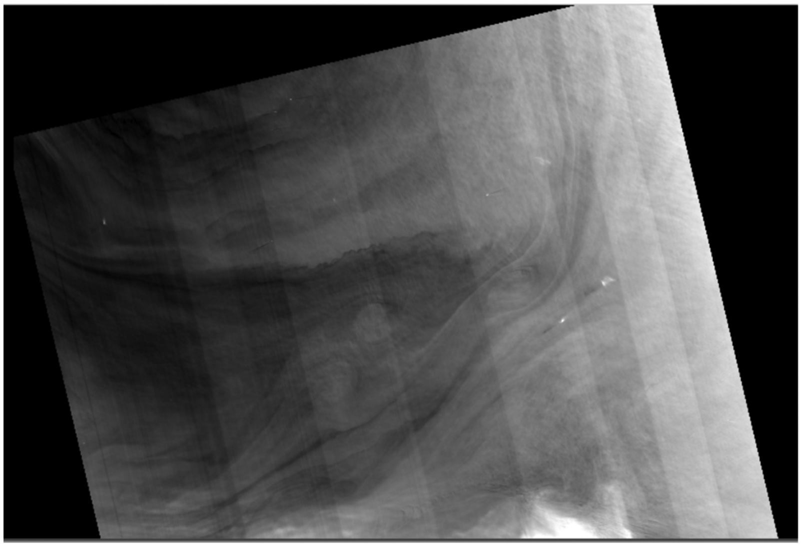

Fig. 1 Striping (high-frequency feature) and Banding (low-frequency feature) uniformity visual artifact example for the OLI Coastal Aerosol band as seen in the subset of the LC91560432024098LGN00 ocean scene.[3] This figure is provided solely as an illustrative example of visual nonuniformity. It is not representative of, nor used as, the basis for the statistical analysis in this work, which draws on hundreds of thousands of Earth scenes spanning a wide range of surface types and signal levels.

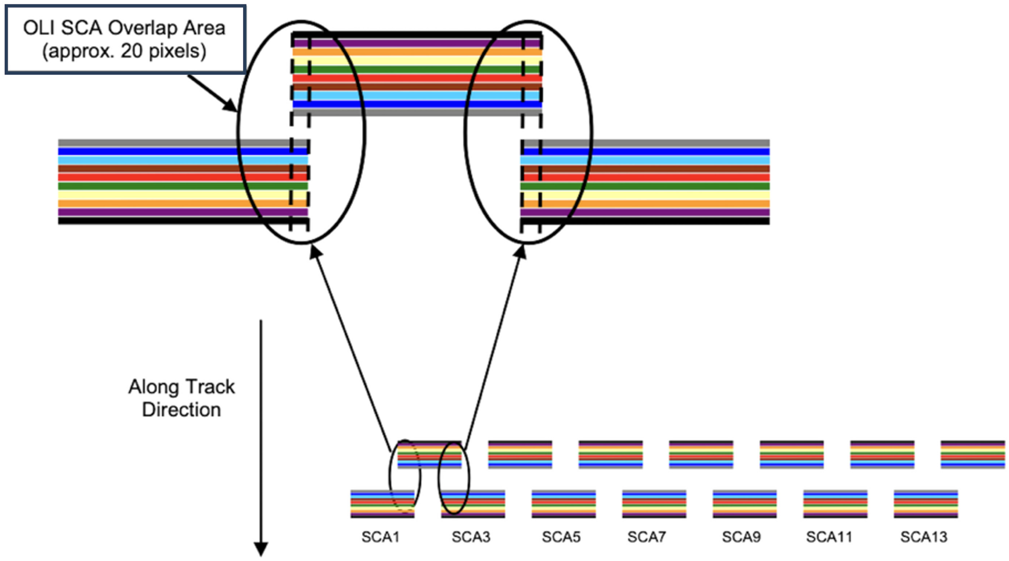

Fig. 2 OLI focal plane layout diagram illustrating overlap between even and odd numbered FPM.[4] Note that the term SCA is used interchangeably with FPM.

contrast-step in the across-track (banding). In the OLI system, this metric is computed at each of the 13 overlap zones within a single spectral band (Fig. 2). Within a single L1T image, for every spectral band, the overlap zone between adjacent FPMs contains thousands of pixel-pair sets that are captured within a few frames in the along-track direction and composed of more than 15 co-registered pixels in the across-track direction. From these sets of spatial-temporal pixel pairs, the mean and standard deviation statistics of ratios or differences are produced for each of the overlap zones in every spectral band. The statistical information produced enables robust trending of this specific uniformity metric at all focal plane boundaries over time.

Building upon the analytical approaches presented in previously cited publications that explored this methodology for uniformity metric evaluation, this study extends the analysis to the Landsat 9 OLI, examining overlap statistic results throughout the mission's operational period. The results presented in this article are based on the USGS Landsat 8 & 9 Collection 2 processing version.[5–7] The analysis uses Earth scene data statistics acquired throughout the Landsat 9 lifetime, which at the time of this publication exceeds four years. The results section presents a comparison of the FPM overlap residual nonuniformity metric derived from two independent sources: (1) operational Earth scene observations and (2) dedicated onboard OLI Solar diffuser calibration collects. This validates the Earth scene methodology against the established Solar diffuser reference. The discussion and future work section of the article describe the potential of this unique Earth-based dataset to become a reference method for robust uniformity metric performance assessment from which calibration coefficients can be derived. The dataset used spans a wide distribution of signal levels and diverse ground types. It should be noted that Earth scenes provide varied BRDF conditions. Hence, they reflect scenarios that existing onboard calibrators cannot evaluate.

This publication presents an approach that uses Earth scene data to assess the on–orbit uniformity performance of the Landsat 9 mission. Earth-scene statistics offer a unique opportunity to evaluate uniformity under true operational conditions, providing complementary—and, in some cases, alternative—information to onboard calibration sources. The analysis characterizes uniformity at specific spatial positions (the focal plane boundary zones) inherent to the OLI focal plane design. It also examines temporal trends extracted from the Earth–based statistics. In L9 OLI and other push broom imaging systems with staggered sensor chip focal plane architectures, the nominal Earth collects to produce co-registered pixels. These co-registered pixels provide overlapping measurements of the same ground target viewed by different detectors. In this report, it is demonstrated that these measurements provide a means to assess uniformity. Furthermore, that assessment is comparable to that achieved with a stable, well-characterized onboard Solar diffuser. The analysis presented here quantifies the long-term stability of these Earth-based overlap statistics and demonstrates their capability to serve as a robust, mission-sustaining uniformity metric, thereby addressing a key gap in uniformity monitoring frameworks for systems with limited or no onboard calibration capabilities. Hence, this report demonstrates that Earth-based scene statistics can effectively support the maintenance of radiometric uniformity in calibrated data products to better than 1% (1–sigma) throughout the mission's operational lifetime.

To provide a clear outline of what follows, the remainder of this article is organized as follows. Section 2 describes the background and general information related to OLI summarizes the Landsat 9 OLI focal plane architecture and the established Solar diffuser calibration framework. Section 3 presents the methodology for the processing steps used to derive overlap statistics from both Solar diffuser collects and Earth scenes, including the filtering and temporal–smoothing strategies applied to the large Earth-scene archive. Section 4 provides the results of the analysis, including long term trending and a comparison between Earth-scene-based and Solar-diffuser-based uniformity assessments. Section 5 discusses the implications of these findings, including the broader applicability of overlap–statistics methods to other staggered push broom imaging systems. Finally, Sec. 6 summarizes the principal findings and outlines the broader applicability of this Earth-scene-based uniformity assessment approach to future missions.

2 Background

The Landsat 9 OLI payload, designed and built by Ball Aerospace & Technologies Corporation (currently BAE Space and Mission Systems) is an optical Earth observing spectral radiometer that utilizes a push broom design to image the Earth in both the visible and near-infrared (VNIR) and short wavelength infrared (SWIR) spectral bands.[8,9] OLI is composed of 14 staggered FPMs, which are Raytheon Vision Systems hybrid chips using silicon (VIS–NIR) and mercury cadmium telluride or HgCdTe (SWIR) detectors bump bonded onto a readout integrated circuit(ROIC).[10,11] The OLI's absolute band average radiometric calibration and the relative per-detector calibration are maintained using the onboard calibration system. Repeatable observations of the stable Solar diffuser panel, as well as shutter collects, enable characterization and trending of per-detector stability and relative response changes, which are updated in the quarterly releases of the calibration parameter files (CPFs).[12,13]

The top of atmosphere (TOA) science product quality is preserved throughout the mission lifetime through these quarterly updates to the relative gains and, at times, the absolute gain parameters.[14] However, throughout its operational period, OLI has exhibited intermittent visible banding and striping artifacts in data products at levels below 0.5% of the signal.[15] Although these artifacts fall below typical data quality specifications, their presence highlights the substantial technical challenge of detecting, characterizing, and correcting residual spatial non-uniformities at sub-percent precision levels.

The concept of using Earth data for uniformity characterization in remote sensing has been extensively documented in the literature. Numerous publications have discussed various numerical approaches for using Earth data to derive and compute detector level relative gain corrections aimed at improving data product uniformity.[16] Two methods have been used for the Landsat missions as validation tools. The first is the histogram equalization approach, which utilizes Earth scenes with high mean signal and low standard deviation.[17] The second method is the 90-deg yaw collects of Earth scenes, which produce approximately co-registered sets between adjacent detectors.[18–20]

A common issue with these methods is that, while they address the uniformity problem from a statistical point of view, they require specific assumptions about scene type and scene uniformity, as well as reliance on the spacecraft's ability to perform a successful yaw steering collect configuration. As a result, the number of scenes available for these analyses is limited.

In contrast, the overlap statistic-based metric illustrates the benefits of applying a mean ratio computation approach to specific detector sets within the focal plane. The focal plane design ensures that this approach produces guaranteed co-registration between detector pairs in every Earth collection (including off-nadir types) for detector sets near the boundaries between FPMs.

The overlap statistic approach avoids many of the restrictive scene characteristic assumptions required by traditional uniformity methods. By comparing co-registered measurements from overlapping detector responses, this methodology can be applied to virtually any operational Earth scene. This enables analysis of a substantially larger dataset than specialized acquisition modes, such as yaw maneuver collect, which require dedicated spacecraft pointing and provide limited temporal sampling.

For a well-corrected, geo-registered science data product, the expected ratio computed for the overlap statistic should be very close to 1 across all overlap zones and for all spectral bands. This should reflect the observations when extracting equivalent results from the radiometrically corrected and angular view BRDF compensated Solar diffuser (SD) panel collects.

Landsat maintains uniformity performance on-orbit using the on-board SD panel collected as the known "flat" reference target, from which the set of relative gain calibration parameters is calculated quarterly. The updated CPF uses results from multiple collects taken in the previous quarter to set the relative gains for the upcoming quarter. With this calibration update approach, the mission has demonstrated that, during nominal operations, the relative gains remain valid for up to two quarters. This relative gain maintenance cadence has been shown to be sufficient for maintaining science product uniformity performance. As designed, the OLI views the SD panel in a fixed 45 deg/45 deg configuration. As a result, the signal profile across the OLI focal plane produces a characteristic response tilt across the focal plane array [Fig. 3(a)]. This pattern is a direct result of the detectors' angular line of sight viewing geometry and the SD panel's BRDF. The resulting signature profile also includes distinct steps between the even and odd FPMs due to the larger along-track angular pointing differences between these modules. The signature response profile for each spectral band is unique and follows the variation of the SD panel reflectance as seen by the OLI detectors across the focal plane.

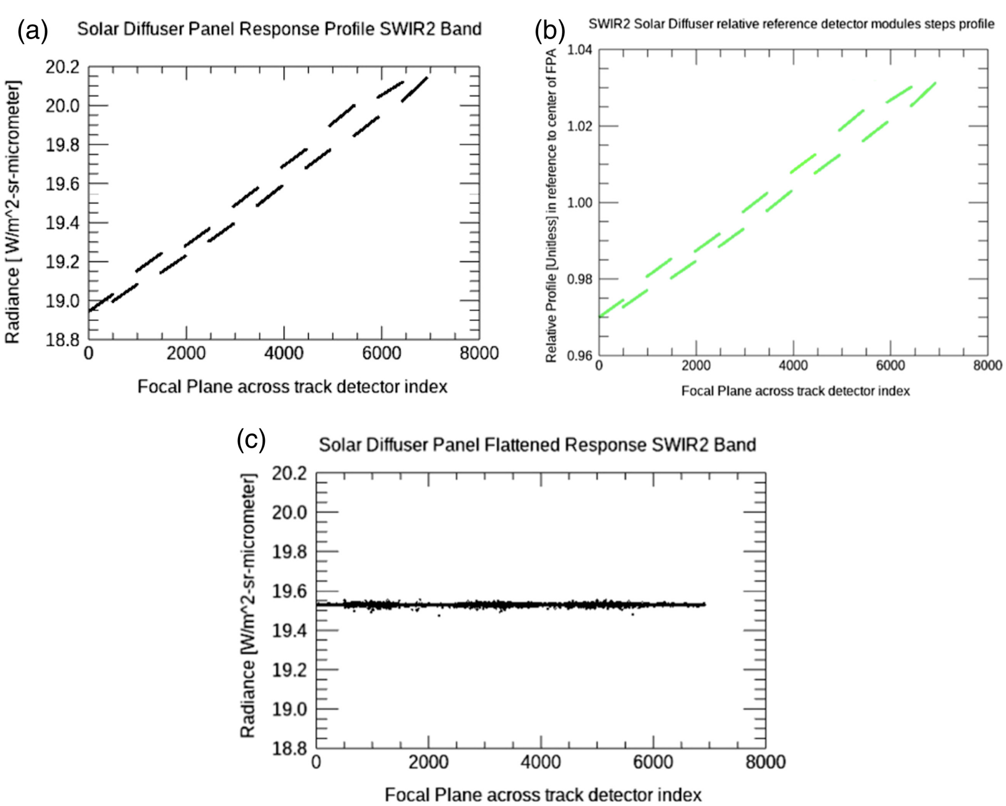

Fig. 3 (a) OLI Solar diffuser Illumination profile in the SWIR2 spectral bands; (b) on-orbit average reference profile step non-uniformity between FPMs as induced by the reflectance BRDF variations; (c) BRDF compensated "flattened" radiance from which the overlap statistic metric can be computed.

The average values of eight early on-orbit SD panel collects are used to produce a reference expected signature profile for each spectral band [Fig. 3(b)]. This normalized reference profile captures the expected nonuniformity factors for each spectral band in the SD panel. Unlike Earth view, which collects a scan a scene, the SD collects observing a static target. Similar to the way relative gain computations are produced from SD collections, the radiance response must be compensated for the SD panel BRDF signature profile. This compensation is applied in each spectral band using the corresponding reference signature profile. By applying this correction, the SD panel BRDF is effectively removed, resulting in a flat, uniform response [Fig. 3(c)] from which the relative gain values are computed.

Once the SD radiance response is flattened by the BRDF compensation step, producing the equivalent overlap statistics metrics from these SD collects requires computing the mean and standard deviation of the ratio and difference for 20 across track detector pairs from two adjacent FPMs for each of the 13 overlap boundary zones. The detector pairs used in computing the SD-based overlap statistics metric are not truly geolocated, co-registered pixel pairs on the SD panel. However, because the SD panel is flat and uniform, it is still possible to compute an equivalent metric. Additional considerations unique to the SD-based results include: (a) the response signal is limited to a relatively narrow and nearly fixed portion of the dynamic range, which naturally reduces the uncertainty from residual nonuniformity, and (b) the viewed spectrum is continuous—similar to the pre-launch calibration sphere source spectrum—but different from Earth scene spectra, which lose their continuum due to atmospheric absorption. The next section describes the steps and methods used to compare the Earth-based overlap statistics metrics with the equivalent metrics computed from the SD collects.

3 Method Description

The value of the mean calibrated radiance-response ratio can be computed either from Solar diffuser collects, which view the uniform diffuser under fixed viewing geometry and repeatable BRDF conditions, or from selected sets of co-registered image pixels that view the same point on the Earth. Although the two input datasets require different handling to produce the same metric for the same overlap zones, the results for both are expected to be close to a ratio of 1. To illustrate the value and validity of the Earth-based overlap statistics metric, the corresponding metric computed from the SD collects is compared with the distilled results extracted from the database of Earth-based overlap statistic measurements.

The primary metric derived from the overlap statistics analysis is the ratio of co-registered detector pair responses within each scene because this ratio can be directly related to the relative gains of the FPMs. Therefore, the comparison focuses on the ratio metric. One form of comparison between the two overlap-ratio datasets evaluates the overall temporal mean and temporal standard deviation for each boundary zone and spectral band, using datasets that follow the quarterly update cadence. This is achieved by applying a 90-day temporal moving-average kernel to the Earth-based data and an 88-day moving-average kernel to the SD-based data. A second comparison examines the detailed temporal trends in the smoothed ratio responses. This analysis highlights the degree to which the Earth-based results track the SD-based results and how well the temporal stability of the ratio metric is maintained and monitored by each approach.

Table 1 summarizes the strengths of each source used to derive the overlap statistic values. The results indicate that combining both sources provides a more complete, balanced, and reliable assessment of the operationally achieved response uniformity across the FPM boundaries.

The Solar diffuser-based overlap statistics offer the advantage of minimizing the influence of collect-level stability and uniformity variations on the resulting overlap statistics ratio evaluation. In contrast, the Earth-based overlap statistics inherently capture the effects of scene-dependent spectral variability, nonuniform signals, and nonlinear detector response due to their derivation from a diverse set of surface reflectance collected across a broad portion of the dynamic range.

Because each source is sensitive to different factors, their complementary characteristics strengthen the case for using a combined assessment. Together, they provide a more complete and operationally meaningful evaluation of uniformity at the FPM boundaries.

Table 1 Contrasting the list of attributes of the two forms of data sources that are used in evaluating the overlap statistics.

Earth based overlap stats	Solar diffuser based overlap stats
Various solar azimuth angles	Fixed solar azimuth angle
Different bidirectional reflectance distribution function (BRDF) conditions	Fixed bidirectional reflectance distribution function (BRDF) conditions
Multiple scene segments with varying signal levels	Signal variation is minimal only due to the seasonality of the Earth–Sun distance.
Results are impacted by signal uncertainty and overall payload stability	Primary absolute and relative gain calibration reference—hence, it can auto compensate for payload stability limitation.
Utilized hundreds of thousands of datasets, from which, after filtering only the good set of scenes and randomly sub-selecting 10 scenes per day results of over 3650 datasets per year. Each scene contains tens of thousands of samples of co-registered detector pairs ratios. It provides statistical robustness.	Limited number of datasets: In 4 years, only 214 datasets had been collected. When in each dataset there are only 512 samples for each detector response ratio.
Atmospheric effects create complex noncontinuous spectral signatures in objects that have different spectral signatures compared with the pre-launch and on-orbit calibration sources	Continuous spectral signature source is viewed
After applied filtering the total number of scenes is 10 or greater per day	At most, one collect is acquired every 8 days.
Offer diverse environmental conditions and real-world validation	Provide high-sensitivity, well controlled datasets

The baseline overlap statistic computation methodology operates on all processed scenes without pre-filtering of input imagery or assumptions about scene characteristics, enabling universal application across all operational Earth observations. However, to obtain realistic results that reflect the actual payload performance, statistical filtering is required to remove outlier results caused by clouds, co-registration anomalies, or other abnormalities occurring in any of the overlap zones. This initial filtering ensures that the results used are valid, as their standard deviations fall within ± 2 sigma of the median standard deviation computed across the entire database. A second filtering step applies a random sub sampling of the database to 10 scenes per day, ensuring that the results are not biased toward specific scene types.

To ensure consistency between the two data sources, the Solar diffuser overlap statistic time series was smoothed using an 11-point moving average kernel, corresponding to the $\sim$88-day quarterly calibration updates interval. This processing allows direct comparison with the Earth-scene results, which applied the 90-day smoothing window.

Steps in processing the Solar diffuser data involve (Fig. 4)

1. Convert the OLI mean detector response to radiance units using the current USGS operational calibration parameters, including the relative gain coefficients, as implemented in the USGS processing system.
2. Apply the spectral band reference signature profile to correct for the SD panel BRDF effects and flatten the radiometric response across all the detectors. This step utilizes the time-invariant reference signature response of each spectral band.
3. Using the flattened radiance response, compute the mean and standard deviation of the response ratio for all Solar diffuser collects across all spectral bands and the FPM boundary zones. For each boundary zone, the response ratio is computed between two sets of N detectors positioned on either side of the boundary. The value of N is selected to match the sampling GSD across all spectral bands; therefore, $N = 20$ for Bands 1 to 7 and 9 (30 m) and $N = 40$ for Band 8 (15 m). The specific detector indices defining each boundary zone depend on the FPM design and the number of detectors in each spectral band.

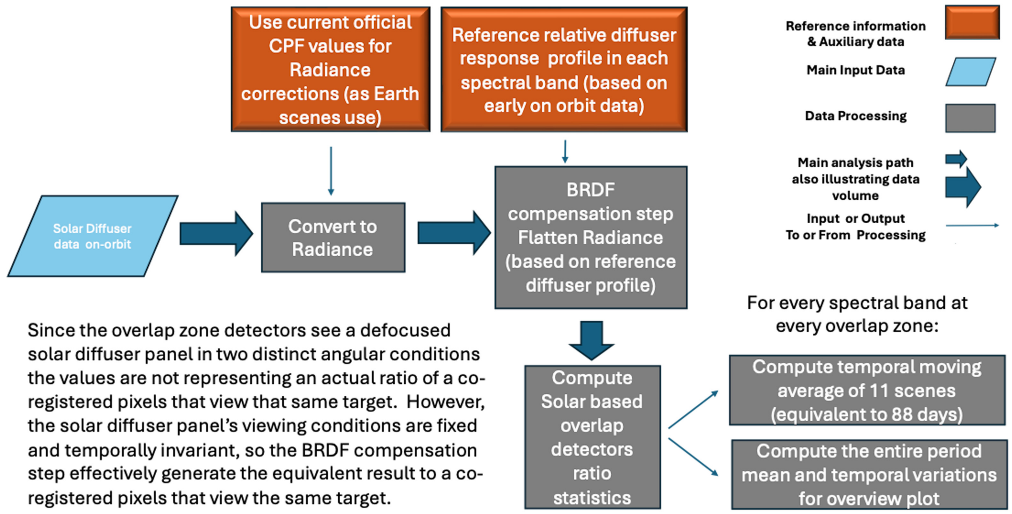

Fig. 4 Block diagram depicting the analysis steps in producing the Solar-based detectors ratio statistics, which are equivalent to the overlap statistic values extracted from the Earth scenes.

The time-invariant signature response used for the BRDF compensation in step 2 was produced from the average response of eight early-mission on-orbit collects. It is the same reference used when computing the on-orbit relative gains. This relative response signature is assumed to be time-invariant because it results from the combined effects of the panel BRDF and the line-of-sight geometry of the focal plane array detectors. Because the line of sight is determined by the telescope optics and the focal plane position, it can be considered time-invariant once the OLI system reaches its steady-state nominal on-orbit operation.

In addition, the BRDF angular characteristics of the panel are also considered nearly time-invariant because the panel is uniformly illuminated by the Sun and maintains its near-Lambertian volume-diffuser properties over time. The invariance of the BRDF angular relationships is not affected by changes in the absolute reflectance of the panel, which will evolve due to use and UV exposure. The reflectance value of the panel is monitored and trended separately through the Solar diffuser panel collections and by comparison to a pristine Solar diffuser panel.

The steps for filtering the Earth overlap statistics data (Fig. 5). Note that the steps presented here do not describe how the database-derived statistics were produced, as that methodology was detailed in a previous publication associated with the algorithm description document for the USGS Image Assessment System.[2]

1. Compute the threshold conditions used to filter only those collections in which the standard deviation of the response ratio, in any band and any overlap zone, falls within the overall median ± 1-sigma threshold (where the median and sigma are computed from all overlap zones and all spectral bands). This filter is designed to remove results affected by clouds, abnormal collection conditions, or unusual artifacts in geometric registration.
2. If any spectral band has even one of the overlap zones that fail the filtering threshold condition defined in step 1, the entire scene is excluded from the set of candidate scenes for random selection. This filtering step reduces the initial set of nearly one million datasets to a few hundred thousand.
3. From the remaining filtered database of scenes, randomly sub-select 10 scenes per day.

The overlap statistic computation methodology operates without pre-filtering of input imagery or assumptions about scene characteristics, enabling universal application across all operational Earth observations. However, to obtain realistic results that reflect the actual payload performance, statistical filtering is required to remove outlier results caused by clouds, co-registration anomalies, or other abnormalities occurring in any of the overlap zones. This initial filtering ensures that the results used are valid, as their standard deviations fall within the range of ± 2 sigma from the median standard deviation computed across the entire database.

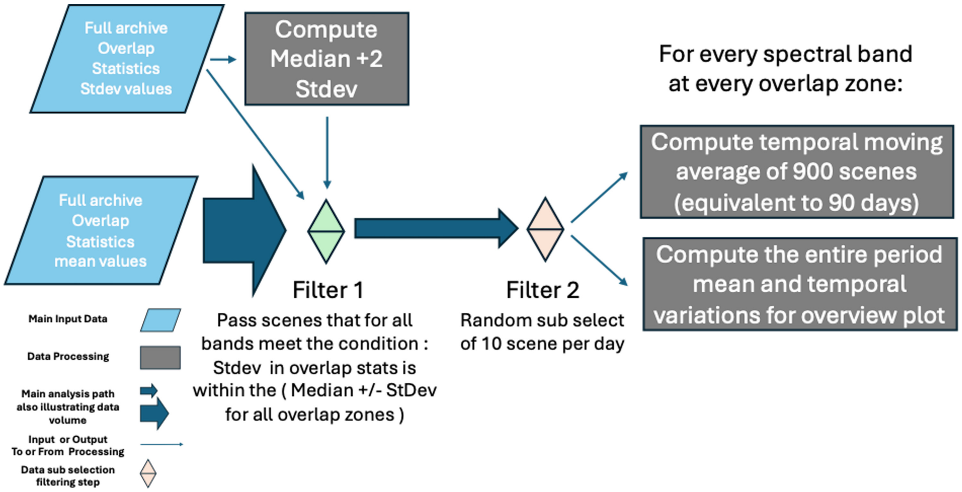

Fig. 5 Block diagram depicting the analysis process of overlap statistics values in the database, illustrating the two filtering steps.

4 FPM Boundaries Overlap Statistics Analysis of Results

The ratio between overlap statistics computed from Earth-based scene observations and the SD-collects-based equivalent results is presented in two formats. The first format presents the plot of the mean ratio value and temporal standard deviation for the entire evaluation period per overlap zone and for all spectral bands (Fig. 6). This offers an overall statistical assessment of the agreement and stability between the two methods. The second format examines the detailed temporal behavior of the ratio across all spectral bands and all FPM boundaries (overlap zones) (Figs. 7 and 8), enabling identification of temporal trends, potential degradation patterns, and time-dependent variations in the correspondence between the methods. To further interpret these temporal behaviors, the analysis incorporates three levels of consistency checks, using the coefficient of variation (expressed in percentage) to assess agreement between the elements evaluated. The first check examines the Earth-based results variations among all overlap zones within a given spectral band [Fig. 7(a)]. The second consistency check examines the Earth-based results between all spectral bands within a single FPM boundary zone [Fig. 7(b)]. Lastly, the third check compares the Earth-based trend for a single band and a single FPM boundary zone with the equivalent Solar-based results (Fig. 8). Combined Figs. 7 and 8 illustrate how a representative a single zone and a single band would be when examining the temporal trends of the two methods.

Before examining the figure-based results in detail, it is important to understand the uncertainties associated with reported values from both methods. The uncertainty estimate for the reported results is computed using the input data provided for the analysis. This data includes the on-orbit Solar diffuser collections and the standard deviation of the Earth-based overlap statistics as computed and stored in the database of the ground system. For this work, the 1-sigma standard-error uncertainty of the Earth-based method is estimated to be up to 0.72% worst case. On the other hand, the standard error of the SD-based is nearly an order of magnitude smaller than the Earth-based results and is estimated to be up to 0.11% in the worst case. This uncertainty variation is one key distinction between the two methods and needs to be kept in mind while viewing the plots in this segment as each of the reported values also holds this extra standard error uncertainty.

The uncertainty associated with the Solar-based results is derived using the quarterly derived per detector relative gain standard deviation that is extracted from the on-orbit SD collects. These standard deviation values are primarily dominated by the system noise and detector stability and also include the quarterly averaging impacts of 11 or more SD collects. These standard deviation values are applied to the standard Taylor's error propagation method for the ratio calculation for every overlap zone. For conservative reporting of the error estimate, the results use the worst-case detector out of 20 detectors within each overlap zone. Lastly, the results are converted to standard error for each overlap zone and for each spectral band by dividing the results with the square root of 20. The number 20 represents the number of detectors averaged at each boundary and follows

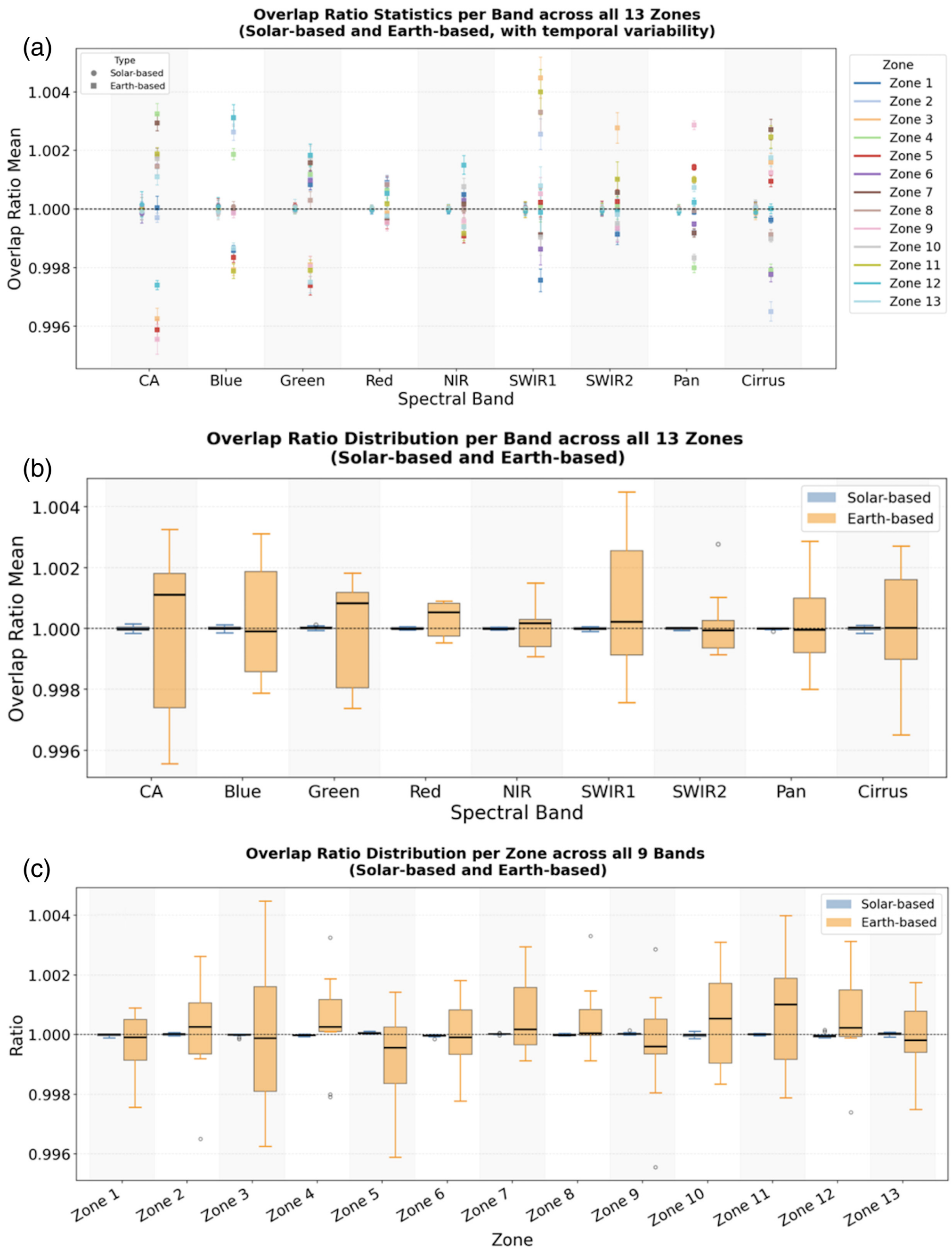

Fig. 6 Comparing between the Earth-based and the Solar based overlap statistics results (a) Overlap statistics ratio values for all FPM boundary zones and all OLI spectral bands, including error bars indicating the temporal variability over the lifetime. (b) Box plot showing the distribution of the overlap-ratio results in each spectral band across the 13 FPM boundary zones with median, range of the zone-means, and extremes. (c) Box plot showing the distribution of the overlap results in each FPM boundary zone across all spectral bands with median, range of the bands means, and extremes.

the processing method for Solar-based overlap statistics (Fig. 4). Worst-case standard error results among all spectral bands and all zones resulted in the value of 0.11% relative to the value for an overlap ratio of 1. For the Earth-based estimate of the uncertainty, the standard error is calculated from the overlap statistics standard deviation values computed for each scene. Because this standard deviation directly reports the overlap ratio error, there is no need to apply the Taylor error propagation step. The standard error computations use the maximum value across all scenes, all bands, and all zones of the standard deviation, and divide it by the square root of 900. The number

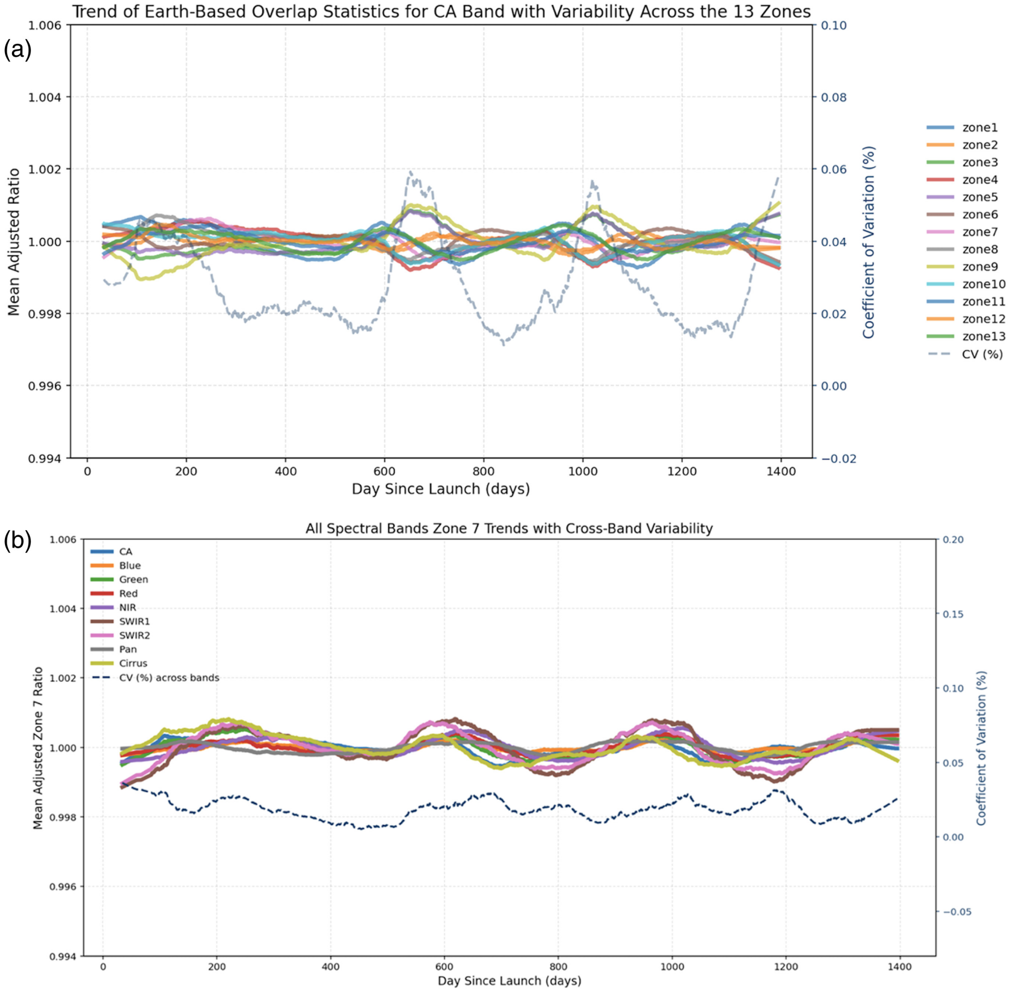

Fig. 7 Mean value adjusted temporal trends of 90 day smoothed Earth-based results. (a) Variation of temporal trend in single spectral band (CA) across all 13 overlap zones along with the coefficient of variation (CV) indicating the percent variation across the 13 zones. (b) Variation of temporal trend in single zone (zone 7 near center of field of view) across all spectral bands along with the coefficient of variation (CV) indicating the percent variation across them.

900 represents the number of scenes used in the 90-day moving average window applied for the produced plots. In that manner, the power of the multiple scenes per day and the quarterly averaging applied is the core element that assists in reducing the error of the Earth-based results.

In the first format, Figs. 6(a)–6(c) provide a multiperspective statistical assessment of the agreement between Solar-based and Earth-based calibration ratios across nine spectral bands and 13 zones over the full evaluation period. Figure 6(a) presents the mean ratios for each spectral band, and error bars represent the temporal standard deviation over the evaluation period, reflecting the stability of each ratio estimate. Minor horizontal offsets are applied between the two marker types to improve readability. Figures 6(b) and 6(c) complement this view through box plot representations that capture the full distribution of ratios, including median, standard deviation, and extremes. In Fig. 6(b), each spectral band contains a pair of box plots that summarize the variability across the 13 zones, enabling a band-by-band comparison of the two calibration approaches. Figure 6(c) reverses this perspective, grouping the box plots by zone to summarize the variability across all 9 spectral bands, offering a zone-level assessment of consistency and potential bias between methods. In both Figs. 6(b) and 6(c), blue boxes correspond to Solar-based ratios and orange boxes to Earth-based ratios. As shown in the plots, and as expected, all Solar-based results are essentially equal to one, exhibiting negligible temporal variation. The Earth-based approach shows consistently small standard deviations from the median across all spectral bands [Fig. 6(c)] and zones [Fig. 6(b)], ranging from 0.05% to 0.27%.

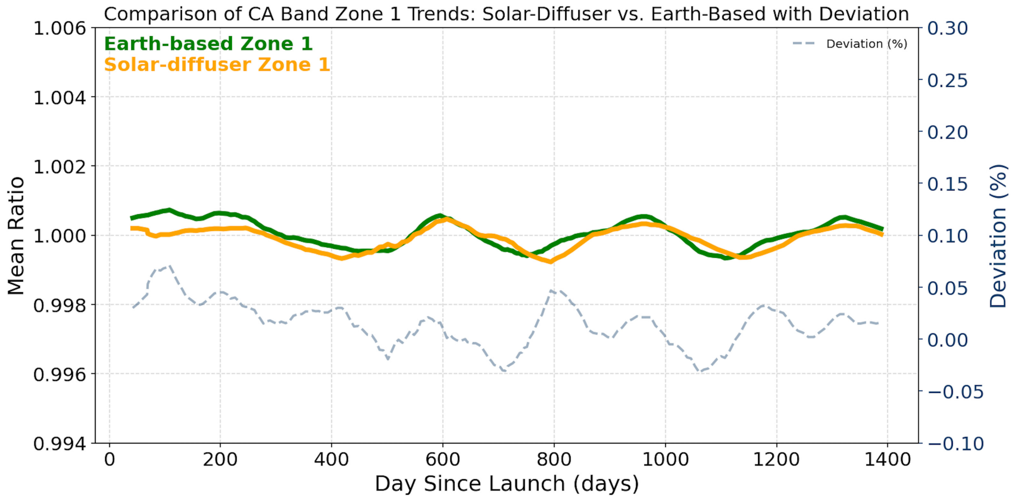

Fig. 8 Comparison of the temporal trends of mean-adjusted CA band overlap statistics ratios for FPM overlap zone 1 (boundary between FPM1 and FPM2), showing 88-day-smoothed Solar-based results and 90-day-smoothed Earth-based results. The percent deviation is the difference between the two with respect to the Solar-based values.

The details of the temporal behavior of the Earth-based ratio across all FPM boundaries are shown in Fig. 7. Figure 7(a) presents the CA band as a representative example, whereas Fig. 7(b) shows zone 7 as a representative case. Both plots also display the coefficient of variation (CV). In Fig. 7(a), the CV represents the variation across the 13 zones for the CA band, and in Fig. 7(b), it represents the variation across all nine bands in zone 7. The selection of these specific spectral bands and zones utilized the distribution information that can be viewed in the corresponding box plots for Figs. 6(b) and 6(c). Although zone 7 does not represent the most challenging conditions, it provides a suitable example of the overall behavior and is likely to be less affected by across-track BRDF variations.

The analysis and results show that both Solar diffuser–based and Earth-based overlap statistics exhibit very small temporal variability across all spectral bands and FPM boundary zones. The plots are produced after normalization that removes the mean offsets computed for each overlap zone and with the application of the 90-day moving average window. The temporal trend variations between the spectral bands revealed that residual seasonal oscillations of the SWIR bands (SWIR1, SWIR2, Cirrus) had the largest peak-to-peak amplitudes of ∼0.15%, while all VIS/NIR bands (CA, Blue, Green, Red, NIR, Panchromatic) remain below 0.1% [Fig. 7(b)]. In this type of figure, the coefficient of variation does not exceed 0.05%, even in the worst-case zone.

The last comparison of the temporal trends of the two methods examines the mission lifetime-derived stability with a direct comparison for the same zone and the same spectral band. Figure 8 plots the temporal stability in the CA band (Band 1) and highlights the comparison between Earth-based results and the SD-based results for zone 1 as an example. The temporal oscillation pattern in the agreement between the Earth-based and SD-based results is not unique to the case shown in Fig. 8. Similar oscillations appear in other spectral bands and overlap zones, typically with slightly larger peak-to-peak amplitudes ranging from 0.2% to 0.4%. These variations remain well below the intrinsic nominal single detector response stability. As seen in Fig. 8 the deviation seen in zone 1 is less than 0.15%, and it is below the Earth-based method uncertainty, which is less than or equal to 0.72%. Therefore, statistically, we can claim that the Earth-based and the SD-based overlap statistics results are indistinguishable because their differences remain below the 1-sigma standard-error uncertainty range.

Taken together, the temporal and statistical results support several key interpretations. One interpretation for the results is that the optimal uniformity observed in the Solar-based evaluation will also repeat in the Earth-based results whenever the OLI instrument acquires a top of atmosphere radiance signal that closely matches both the signal level and the continuous spectral signature measured during Solar illuminated SD panel collects. In practice, however, atmospheric spectral transmission and scene content modify the spectral signature of Earth observations, preventing these conditions from being fully reproduced, particularly in the SWIR spectral bands (SWIR1, SWIR2, Cirrus). Consequently, the Earth-based results exhibit greater variability in the residual ratio across the focal plane array, and this variability is spectrally dependent [Fig. 6(b)].

For a given spectral band, two distinct components of variability are evident: (1) the separation between the even and odd overlap zones and (2) the spread within each cluster of even or odd overlap zones. These behaviors arise from the combined influence of the BRDF characteristics of the observed Earth scenes and the spectral signatures shaped by atmospheric transmission, together with the dominant scene types present in the filtered scene subset used in the analysis. The red and NIR bands demonstrate tight residual nonuniformity, remaining below ±0.2% for all FPM boundaries, whereas several other spectral bands exhibit residuals approaching ±0.4%. These levels of residual nonuniformity are consistent with the minor uniformity artifacts observed in the corresponding Earth image products.

Overall, the analysis across both methods and all spectral bands and zones demonstrates that the observed oscillations and residual nonuniformities derived from Earth-based overlap statistics, generally less than 0.4%, are small relative to instrument uncertainties and confirm that long-term uniformity requirements are consistently maintained throughout the mission. In addition, the results demonstrate that calibration derived from the Solar diffuser panel, when applied to Earth scene data, can yield a low level of reduced uniformity; however, this reduction remains within ± 0.4% in the worst case. Because the plot encompasses information from the full mission lifetime dataset, it also verifies that the uniformity performance is maintained within the expected 0.5% level throughout the mission.

The Earth-based statistics, when combined with the SD collections information, can further improve FPM boundary uniformity by adjusting calibration parameters so that both Solar based and Earth-based assessments exhibit consistent non-uniformity levels. More importantly, the results indicate that the Earth-based overlap statistics, due to their temporal stability, can serve as an alternative source for deriving uniformity correction parameters at the FPM boundaries. Furthermore, in situations where a Solar diffuser is not present or is otherwise unavailable, the Earth-based overlap statistics can be used to characterize nonuniformity and derive calibration parameters. As demonstrated in the Landsat 9 OLI results, applying this approach to OLI would not introduce a uniformity deviation exceeding ±0.5%.

5 Discussion and Future Analysis

The integration of detector-to-detector overlap statistics into the Landsat product generation system has proven to be an effective method for monitoring radiometric uniformity. Even without applying BRDF corrections, these statistical trends enable the detection of subtle radiometric calibration changes with a sensitivity better than ±0.7%. This level of sensitivity reflects both the inherent variability of the assessment methodology and the maximum observed error under worst-case conditions. Furthermore, the normalized long-term trend of the overlap statistics reveals even smaller (±0.1%) and repeatable seasonal variations that are consistent with results obtained from the Solar diffuser–based analysis. Achieving such robust Earth–scene–based assessments requires access to a large collection of observation statistics at subsets of the focal plane spatial positions. For example, in this work spanning nearly four years of Landsat 9 OLI operations, stringent filtering to ensure reliable uniformity assessment reduced an initial archive of more than half a million scenes to a final sample of 12,590.

Although use of an onboard calibration device such as the Solar diffuser panel offers the distinct advantage of controlled, stable, and well-characterized measurement conditions with fixed BRDF geometry, these datasets are typically less frequent and more limited than the vast daily set of Earth collects. Uniformity assessment results derived from the onboard diffuser eliminate variability associated with scene characteristics, atmospheric conditions, and temporal surface changes, thereby isolating the purely instrumental detector-to-detector consistency. In contrast, Earth-scene-based overlap statistics naturally span the full operational radiometric dynamic range and incorporate effects of relative spectral response variability, signal-dependent nonlinearity, and natural scene diversity. Hence, a complete assessment of focal plane module nonuniformity requires the combined use of both Earth-scene- and calibration-device-based analyses, providing the most comprehensive characterization of detector uniformity under both controlled and operational conditions. Although the diffuser ensures uniform response under controlled BRDF conditions, Earth scenes introduce atmospheric and BRDF variability that result in slightly less uniform behavior, as shown in Sec. 4. The observed split between odd and even overlap zones, and differences among spectral bands, are consistent with uncompensated BRDF effects. This was confirmed by evaluating diffuser-based overlap statistics without BRDF correction. Hence, it is expected that applying BRDF compensation to the Earth-based statistics would be expected to further align the two methodologies.

Although dependent on large volumes of Earth-scene data and careful filtering, the overlap statistics framework holds strong potential for enhancing the characterization of data products, including seasonal nonuniformity compensation, improved nonlinearity corrections, and evaluation of cross–calibration between the Landsat 8 and Landsat 9 OLI instruments in the context of their nonuniformity attributes. Such additional analysis will require customized development steps that link the baseline results to the attributes being quantified. For example, refinement of focal plane module residual nonlinearity can be achieved by binning overlap statistics by signal level, requiring only modest customization of the filtering steps illustrated in Fig. 5. Converting overlap statistic results into FPM gain adjustments further requires establishing a regression analysis that quantifies the correlation between the two.

Although the Earth-scene approach performs well for Landsat 9 OLI, its effectiveness benefits significantly from the instrument's intrinsic stability, including highly stable detectors and exceptionally tight sub-pixel geometric registration and geodetic accuracy—typically on the order of one-tenth of a pixel. The general methodology of Earth-based overlap statistics, however, is applies to other pushbroom sensors with similar focal plane architectures. For systems with lower radiometric or geometric stability, uniformity assessments or subsequent corrections may exhibit larger residuals. Most importantly, for systems that do not include an onboard calibration device, this approach could serve as a valuable substitute to help maintain data product uniformity.

6 Conclusion

This article presents the results of the overlap statistics analysis for Landsat 9 OLI, demonstrating how the alternative Earth scene data approach can be used to quantitatively evaluate radiometric uniformity over the mission lifetime. Although Landsat 9 was used in this study, which demonstrated the highest performance achievable with this approach, the method is broadly applicable to other push broom sensors featuring staggered focal plane architectures. Reliable response ratio extraction from overlapping detectors requires a large archive of Earth scenes and robust filtering within the analysis. The assessment can be applied to the full range of signal levels or customized to specific signal levels or other scene attributes through tailored processing filters. As such, this method can serve as a valuable backup validation—or potentially a primary approach—for monitoring relative gains, especially when onboard calibration devices are limited.

Future adoption of this method as a primary monitoring tool will require some additional preparations that tailor the analysis to the system's temporal stability, baseline calibration uncertainty, and revisit cadence of Earth sites. It would require, at minimum, an initial analysis of at least one year of Earth scenes, while subsequent monitoring would rely on smaller sets of frequently revisited scenes that represent annual statistics and the temporal stability of the results.

The Landsat 9 OLI results illustrate how a strong stability of the payload assists the overlap statistics analysis. For OLI, this study shows that the availability of co-registered pixels enables monitoring of on-orbit performance and product uniformity with a sensitivity better than $\pm 1\%$. Such a level of stability is challenging to characterize in either absolute or relative terms and difficult to achieve even during prelaunch calibration and characterization tests. Temporal analysis shows small, repeatable seasonal variations in the response ratios. These variations, on the order of 0.1%, are consistent with those observed in Solar-diffuser-based analyses. This small level of variation is insignificant, as it is roughly half the known detector response standard deviation. The strong agreement between the Earth scene and Solar diffuser results indicates a common underlying driver and reinforces the robustness and reliability of the on-orbit calibration. Together, these results confirm that overlap statistics analysis provides a stable, high-fidelity means of tracking radiometric uniformity on-orbit, offering strong confidence in the long-term consistency and scientific reliability of the Landsat 9 OLI data record.

Disclosures

This research received no external funding; hence, the authors declare that there are no financial interests, commercial affiliations, or other potential conflicts of interest that could have influenced the objectivity of this research or the writing of this paper.

Code and Data Availability

- Part of the data presented in this article is available in the article as well as public websites referenced in the article.
- Parts of the data shown related to OLI2 calibration source collection or the Earth-based statistics may only be available on request due to restrictions.

Acknowledgments

All of the authors were involved in the various aspects of the radiometric scale assessment pre-launch and on-orbit. R.L.: writing and data extraction of detector overlap statistics and related analysis. C.T.P. and J.A.M.: reviewed the edited results, plots, tables. K.J.T.: NASA Landsat Cal/Val managers, reviewed the analysis results and guided the team. R.L. and J.A.M.: processed the OLI data and conducted radiometric characterization of Solar diffuser data. All authors have read and agreed to the published version of the manuscript. The authors used Microsoft 365 Word Copilot to assist with grammar correction, language refinement, and editorial suggestions. All scientific content, analysis, and conclusions were developed by the authors.

References

1. R. Levy et al., "Landsat 8 Operational Land Imager (OLI) detector-to-detector uniformity challenge and performance," *Proc. SPIE* **9218**, 921818 (2014).
2. Department of the Interior, U.S. Geological Survey, "Landsat 8-9 calibration and validation (Cal/Val) algorithm description document (ADD)," Version 5.0, March 2025, EROS, Sioux Falls, South Dakota, https://d9-wret.s3.us-west-2.amazonaws.com/assets/palladium/production/s3fs-public/media/files/LSDS-1747_Landsat8-9_Calibration-Validation_Algorithm-Description-Document_v5.pdf (accessed March 30, 2026).
3. Department of the Interior, U.S. Geological Survey, "Landsat 8 (L8) data users handbook," Version 5.0, November 2019, pp. 79–81, https://d9-wret.s3.us-west-2.amazonaws.com/assets/palladium/production/s3fs-public/atoms/files/LSDS-1574_L8_Data_Users_Handbook-v5.0.pdf (accessed March 30, 2026).
4. Department of the Interior, U.S. Geological Survey, "Landsat 8 (L8) level 0 reformatted (L0R) data format control book (DFCB)," Version 15.0, February 2017, https://d9-wret.s3.us-west-2.amazonaws.com/assets/palladium/production/s3fs-public/atoms/files/LSDS-750_Landsat8_Level-0-Reformatted_DataFormat ControlBook-v15.pdf (accessed March 30, 2026).
5. U.S. Geological Survey, "Landsat collection 2," https://www.usgs.gov/landsat-missions/landsat-collection-2 (accessed March 30, 2026).
6. Department of the Interior, U.S. Geological Survey, "Landsat 8-9 Operational Land Imager (OLI) – thermal infrared sensor (TIRS) collection 2 Level 1 (L1) data format control book (DFCB)," Version 7.0, March 2025, https://d9-wret.s3.us-west-2.amazonaws.com/assets/palladium/production/s3fs-public/media/files/LSDS-1822_Landsat8-9-OLI-TIRS_C2_L1_DataFormatControlBook-v7.pdf (accessed March 30, 2026).
7. "Landsat Collection 2 Level–1 Data," https://www.usgs.gov/landsat-missions/landsat-collection-2-level-1-data (accessed March 30, 2026).
8. NASA, "Landsat 9 mission details," https://science.nasa.gov/mission/landsat-9/mission-details/ (accessed March 30, 2026).
9. NASA, "Landsat 8 Operational Land Imager (OLI)," https://science.nasa.gov/mission/landsat/oli/ (accessed March 25, 2026).
10. E. J. Knight and G. Kvaran, "Landsat–8 Operational Land Imager design, characterization and performance," *Remote Sens.* **6**(11), 10286–10305 (2014).
11. K. Lyndhal et al., "Summary of the operational land imager focal plane array for the Landsat Data Continuity Mission," *Proc. SPIE* **8155**, 81550Y (2011).
12. U.S. Geological Survey, "Landsat calibration parameter files," https://www.usgs.gov/landsat-missions/landsat-calibration-parameter-files (accessed March 30, 2026).
13 U.S. Geological Survey, EROS CalVal Center of Excellence (ECCOE), "ECCOE Landsat quarterly calibration and validation reports," https://www.usgs.gov/calval/eccoe-landsat-quarterly-calibration-and-validation-reports (accessed March 30, 2026).
14. National Geospatial Advisory Committee, Landsat Advisory Group, "Landsat data: community standard for data calibration," A Report of the National Geospatial Advisory Committee, October 2020, p. 12, https://

www.fgdc.gov/ngac/meetings/october-2020/ngac-paper-landsat-data-community-standard-for.pdf (accessed March 30, 2026).
15. M. O. Haque et al., "ECCOE Landsat quarterly calibration and validation report—Quarter 3, 2025," U.S. Geological Survey Open–File Rep. 2026–1069, p. 55 (2026).
16. U.S. Geological Survey, "Landsat calibration notices," https://www.usgs.gov/landsat-missions/landsat-calibration-notices (accessed March 30, 2026).
17. C. Anderson, D. L. Helder, and D. Jeno, "Statistical relative gain calculation for Landsat 8," *Proc. SPIE* **10402**, 104021F (2017).
18. C. Begeman et al., "Relative radiometric correction of pushbroom satellites using the yaw maneuver," *Remote Sens.* **14**(12), 2820 (2022).
19 C. Anderson et al., "Radiometric correction of RapidEye imagery using the on–orbit side–slither method," *Proc. SPIE* **8180**, 818008 (2011).
20. L. Gopan et al., "Scene based non–uniformity correction for optical remote sensing imagery," *Int. J. Image Graph. Signal Process.* **9**(12), 50–57 (2017).

Raviv Levy is a chief optical engineer at Science Systems and Applications, Inc. (SSAI), supporting the Landsat mission at NASA Goddard Space Flight Center for over 20 years. He received his BS and MS degrees in optical sciences from the University of Arizona Optical Science Center in 1998 and 2000, respectively. He has authored numerous SPIE proceedings and journal papers. His research interests include pre-launch and on-orbit calibration, including stray light, ghosting, nonlinearity, nonuniformity, and spectral response characterization.

Cibele Teixeira Pinto received her MS and PhD degrees in remote sensing from INPE, Brazil, in 2011 and 2016. She was an image engineer at the SDSU Image Processing Laboratory from 2017 to 2024. She is currently a lead research scientist at SSAI, supporting Landsat calibration/validation at NASA Goddard. Her research interests include vicarious radiometric calibration, satellite intercalibration, and uncertainty analysis in calibration processes.

Jeffrey A. Miller received his BS degree from the University of Maryland in 1994. He is a lead scientific programmer/analyst at SSAI, supporting Landsat calibration/validation at NASA Goddard. His work focuses on algorithm development for calibration data analysis. He has developed remote-sensing-based algorithms for sea ice melt and freeze detection. His interests include calibration support, algorithm testing, data product improvement, and instrument performance monitoring.

Kurtis Thome received his BS degree from Texas A&M University and his MS and PhD degrees in atmospheric sciences from the University of Arizona. He is a physical scientist at NASA Goddard Space Flight Center. He has served in key calibration roles for Landsat and Climate Absolute Radiance and Refractivity Observatory (CLARREO) missions. He is currently Terra project scientist, calibration lead for Landsat 8 and 9, deputy calibration lead for Landsat 10, and VIIRS Instrument Scientist.